Natural Resources for Human Health
eISSN: 2583-1194

Original Research

Received 18 July 2026
Revised 25 Aug 2026
Accepted 10 Sep 2026

Natural Resources for Human Health 2026, Vol. 6 (22s): 510–522

KEYWORDS:
Citrus aurantiifolia, chronic wounds, molecular docking, molecular dynamics, TNF-α, MMP-9.

In Silico Study of Non-Volatile Compounds from Citrus aurantiifolia Peels Targeting MMP-9and TNF-α in Chronic Wound Management

Imam Adrian Rakhman[1]*, Syahrijuita Kadir[2], Marhaen Hardjo[3], Ilhamuddin[4], Gita Vita Soraya[5]

[1]Department of Biomedical Sciences, Graduate School, Hasanuddin University, Makassar, South Sulawesi, Indonesia
[2-5]Department of Biochemistry, Faculty of Medicine, Hasanuddin University, Makassar, South Sulawesi, Indonesia

ABSTRACT: Chronic wounds represent a major clinical problem characterized by persistent inflammation and excessive degradation of the extracellular matrix mediated by TNF-α and MMP-9. The aim of this study was to identify non-volatile compounds from Citrus aurantiifolia (lime) peel as potential inhibitors of these two therapeutic targets for topical application. Phytochemicals were filtered in silico according to physicochemical "minimum requirements" for skin penetration (MW <500 Da, Log P 1–5) and safety profiles (AMES toxicity and skin reaction). Molecular docking against MMP-9and TNF-α, followed by 50 ns molecular dynamics (MD) simulations, was performed to evaluate binding interactions and complex stability. 3'-Hydroxygenkwanin (−10.1 kcal/mol) and luteolin (−10.0 kcal/mol) exhibited particularly favorable predicted binding affinities for MMP-9, whereas obacunone and limonin showed more favorable dual-target binding profiles (−9.1 to −10.3 kcal/mol) than doxycycline (−7.6 kcal/mol for MMP-9and −8.0 kcal/mol for TNF-α). Docking analysis showed interactions with important residues, including His226 in MMP-9and Tyr119 in TNF-α. The structural stability of the 3'-hydroxygenkwanin and luteolin complexes with MMP-9, as well as the obacunone, luteolin, and limonin complexes with TNF-α, was supported by MD simulations. In conclusion, 3'-hydroxygenkwanin represents a promising MMP-9-targeting candidate, while obacunone and limonin show particularly promising dual-target binding profiles. These findings support selected C. aurantiifolia phytochemicals as potential lead candidates for further investigation in topical chronic wound management.

1. INTRODUCTION

Wound healing is a complex and highly coordinated physiological process that can be divided into four overlapping stages: hemostasis, inflammation, proliferation, and remodeling (1). The inflammatory phase is an important defense mechanism, which involves various immune cells at the injury site to clear pathogens and cellular debris (2). However, if the inflammatory response is dysregulated or prolonged, the wound will not advance into the proliferative phase and will become chronic and non-healing (3). These chronic wounds are defined by a hostile microenvironment of persistent oxidative stress and tissue damage, which is a major clinical challenge worldwide. A central factor in this pathological cycle is the biochemical relationship between tumor necrosis factor-alpha (TNF-α) and matrix metalloproteinase-9 (MMP-9) (4,5).

TNF-α is a key pro-inflammatory cytokine that acts as a signaling trigger for the overexpression of MMP-9, which is responsible for the degradation of the extracellular matrix (ECM) (6). Although tightly controlled MMP-9activity is essential for tissue remodeling, increased TNF-α levels promote overabundant MMP-9activity and unregulated breakdown of freshly formed

collagen and growth factors (5,7). This destructive synergy prevents the structural stabilization of the wound bed, thus the simultaneous inhibition of both TNF-α and MMP-9is a critical therapeutic strategy to restore the healing trajectory.

Pharmacological treatment of complex wounds is necessary, but conventional commercial topical agents often have significant clinical disadvantages. Some synthetic treatments, such as certain broad-spectrum antibiotics and corticosteroids, have been associated with adverse effects, including skin thinning, delayed re-epithelialization, and the growing problem of drug resistance (8,9). These limitations emphasize the critical need to develop safer and biocompatible alternatives that can provide multi-target therapeutic effects without compromising the skin barrier integrity.

Natural resources have become one of the top sources for drug discovery because of their diverse bioactive profiles and generally better safety margins (10). Phytochemicals such as flavonoids, limonoids, and phenolic compounds possess inherent anti-inflammatory, antioxidant, and tissue-regenerative characteristics that can modulate the wound microenvironment (11–13). Peels of C. aurantiifolia are such valuable resources because they are rich in non-volatile constituents, such as 3'-hydroxygenkwanin, luteolin, and different furanocoumarins (14,15).

Therefore, in silico studies are important for the systematic screening and identification of specific inhibitors from these lime peel derivatives that effectively target MMP-9and TNF-α. Computational techniques enable the precise evaluation of molecular binding affinities and the screening for the rigorous physicochemical properties for topical penetration, such as a molecular weight below 500 Da and an ideal Log P value of 1 to 5 (1, 2, 8). This study aims to find potential non-volatile compounds from C. aurantiifolia to see their wound-healing potential by blocking MMP-9and TNF-α.

2. MATERIALS AND METHODS

2.1 Study Material

Hardware

The molecular docking and molecular dynamics investigations were performed on a custom-built workstation equipped with the following specifications: 64 GB of random-access memory (RAM), a single Intel Core i7-13900K processor, an NVIDIA RTX 3090 graphics processing unit (GPU), and a dual system with Ubuntu 22.04 LTS and Windows 11 Pro-64-bit.

Software

This study utilized several software tools to investigate the activities of compounds derived from *C. aurantiifolia*. Phytochemical data sources and compound selection criteria were established based on comprehensive literature profiling of major active constituents in *C. aurantiifolia* peel extracts combined with initial drug-likeness screening (adhering strictly to Lipinski's Rule of Five, molecular weight < 500 g/mol, and optimal log P parameters).

The 3D structures and chemical optimizations were edited using the ChemDraw package (16). Macromolecular receptor preparation and minimization were performed using UCSF Chimera 1.18. Binding affinities and virtual screening were analyzed using PyRx 0.8 (19). Intermolecular interactions and complex trajectories were visualized using Discovery Studio Visualizer 2021 and PyMOL 3.1 Free Edition (17). Ligand format conversions were executed via Open Babel, while SwissParam was utilized for topology generation. Molecular dynamics simulations were carried out using open-source GROMACS 2025.3.

2.2 Ligand Retrieval and Optimization

All phytochemical compounds derived from *Citrus aurantiifolia* peels were retrieved in 3D .sdf format from the PubChem database (https://pubchem.ncbi.nlm.nih.gov/). Geometric optimization of all isolated ligands was performed using Avogadro 1.2.0, applying the MMFF94s force field and the conjugate gradient algorithm to reach energy minima. The optimized ligand structures were subsequently converted into AutoDock-compatible .pdbqt format using AutoDockTools.

2.3 Protein Receptor Preparation

The three-dimensional crystal structures of Matrix Metalloproteinase-9 (MMP-9; PDB ID: 4XCT) and Tumor Necrosis Factor-alpha (TNF-α; PDB ID: 2AZ5) were downloaded from the RCSB Protein Data Bank (https://www.rcsb.org) in .pdb format. Discovery Studio Visualizer 2021 was utilized to strip non-catalytic ligands, non-essential heteroatoms, and crystallographic water molecules beyond 4 Å from the active binding pocket.. Essential structural and catalytic cofactors, specifically the catalytic Zn^{2+} ion in MMP-9, were strictly retained to preserve the structural integrity of the active binding site. Co-crystallized native

ligands were isolated for subsequent re-docking validation. Missing residues, hydrogen atoms, protonation states at physiological pH (7.4), and Gasteiger charges were assigned using the "Dock Prep" module in UCSF Chimera 1.18.

2.4 Virtual Screening and Pharmacokinetic (ADMET) Profiling

Physicochemical characteristics, drug-likeness parameters, and pharmacokinetic profiles relevant to topical wound healing formulations—including lipophilicity (log P), molecular weight (MW), AMES mutagenicity, and potential skin sensitization—were predicted using the ADMET-AI web platform (https://admet.ai.greenstonebio.com/) (18).

2.5 Molecular Docking and Dynamics Simulations

2.5.1 Molecular Docking Protocol

Blind molecular docking simulations were executed using the AutoDock Vina algorithm embedded within the PyRx 0.8 software suite (19). To explore all potential binding sites on the receptor surface, a blind docking approach was applied by setting the grid box dimensions to 40 × 40 × 40 Å^3 centered on the geometric center of the macromolecular structures for both MMP-9 and TNF-α, effectively covering the active binding cavities and surrounding domains. The exhaustiveness parameter was set to 8 to ensure a thorough conformational search.

Ligand-protein complexes resulting from the docking procedure were exported and converted into .mol2 format via Open Babel, with explicit polar and non-polar hydrogens generated. Topologies for the high-affinity complexes were produced using the SwissParam server based on the Merck Molecular Force Field (MMFF) framework.

2.5.2 Molecular Dynamics (MD) Simulations

Molecular dynamics (MD) simulations were performed using GROMACS 2025.3 utilizing the CHARMM27 force field and the single point charge (SPC) explicit water model. The protein-ligand complexes were immersed in a periodic cubic solvation box with a minimum solute-box wall distance of 1.0 nm and neutralized by adding counterions (Cl^- or Na^+). System energy was minimized over 5,000 steps using the steepest descent algorithm to remove atomic steric clashes.

Subsequently, 100 ps of NVT (constant number of particles, volume, and temperature) and 100 ps of NPT (constant number of particles, pressure, and temperature) equilibrations were conducted at 300 K (using V-rescale temperature coupling) and 1 bar (using Parrinello-Rahman pressure coupling), respectively. Production MD runs were carried out for 50 ns under isothermal-isobaric conditions with a 2 fs time step.

Trajectories were compiled and analyzed to evaluate the structural stability and dynamic behavior of the protein-ligand complex through root-mean-square deviation (RMSD) of backbone atoms, root-mean-square fluctuation (RMSF) of amino acid residues, radius of gyration (Rg) for structural compactness, and intermolecular hydrogen bond counts across the simulation timeline (20,21).

3. RESULTS AND DISCUSSION

3.1 Compounds screening

All compounds found in C. aurantiifolia were first examined for their properties as topical agents by looking at their molecular weight and logP (14,15). The primary barrier of the skin, the stratum corneum (SC), must be properly penetrated by candidate molecules that fulfill certain physicochemical "minimum requirements" to ensure adequate penetration (22). Based on the results in **Table 1**, the screening process targets compounds with a molar mass of less than 500 g/mol to achieve optimal diffusivity and balanced lipophilicity, specifically a Log P between 1 and 5, ideally between 1 and 3 (22). This balance is important, as a molecule must have enough lipophilicity to partition into the lipid-rich SC but enough hydrophilicity to diffuse into the aqueous viable epidermis and dermis (23). Furthermore, safety indicators such as AMES toxicity (mutagenicity) and probability of skin reaction are analyzed in Table 1 to verify that identified compounds do not produce adverse effects like allergic contact dermatitis upon topical application (24,25).

Natural Resources for Human Health
eISSN: 2583-1194

Table 1. Screening of active compounds of *C. aurantiifolia*.

Compounds	MW	LogP	AMES	Skin reaction
methyl isolimonate acetate	544.597	3.3167	0.39	0.30
limonin	470.518	3.1374	0.26	0.32
luteolin	286.239	2.2824	0.58	0.88
3`-hydroxygenkwanin	300.266	2.5854	0.66	0.75
myricetin	318.237	1.6936	0.46	0.89
europetin	332.264	1.9966	0.59	0.80
D-Aspartic acid	133.103	-1.127	0.18	0.29
N-Oxalylglycine	147.086	-1.7282	0.05	0.53
2-(Methylthio)benzothiazole	181.285	3.0182	0.25	0.88
Melibiose	342.297	-5.3972	0.17	0.27
3-Pyridinecarboxaldehyde	107.112	0.8941	0.04	0.70
Synephrine	167.208	0.645	0.04	0.52
2,5-Dihydroxy benzaldehyde	138.122	0.9103	0.36	0.86
trans-Aconitic acid	174.108	-0.4433	0.04	0.73
Citric acid	192.123	-1.2485	0.06	0.31
Adenosine	267.245	-1.98	0.75	0.46
2,3-Desisopropylidenetopiramate	299.301	-2.1937	0.84	0.46
Phenprobamate	179.219	1.7145	0.27	0.53
Stachydrine	143.186	-1.0249	0.00	0.87
Isoorientin	448.38	-0.2027	0.61	0.34
Lactobionic acid	358.296	-5.6689	0.02	0.15
Engeletin	434.397	0.3325	0.62	0.23
trans-3-Coumaric acid	164.16	1.49	0.03	0.47
cis-3-Coumaric acid	164.16	1.49	0.04	0.46
Quercetin	302.238	1.988	0.56	0.89
Isovitexin	432.381	0.0917	0.55	0.30
Rutin	610.521	-1.6871	0.60	0.21
Quercetin 3'-methyl ether	316.265	2.291	0.55	0.76
Isorhoifolin	578.523	-1.0983	0.53	0.18
Narirutin	580.539	-1.1652	0.39	0.13
Narcissoside	624.548	-1.3841	0.54	0.17
Diosmin	608.549	-1.0897	0.52	0.17
Hesperetin	302.282	2.5185	0.57	0.50
Hesperidin	610.565	-1.1566	0.32	0.10
Neohesperidin	610.565	-1.1566	0.32	0.10
Hyperin	464.379	-0.5389	0.64	0.32
Isorhamnetin 3-O-glucoside	478.406	-0.2359	0.57	0.22
Syringetin 3-glucoside	508.432	-0.2273	0.47	0.21
Mono-2-ethylhexyl phthalate	277.34	2.4233	0.01	0.40

Scoparone	206.197	1.8102	0.18	0.16
Heraclenin	286.283	3.0954	0.61	0.37
2',6'-Dihydroxy-4-methoxychalcone-4'-O-neohesperidoside	594.566	-0.967	0.45	0.19
Oxypeucedanin hydrate	304.298	2.0498	0.19	0.11
Byakangelicol	316.309	3.104	0.67	0.36
7-Methoxycoumarin	176.171	1.8016	0.17	0.19
Angelicin	186.166	2.5392	0.28	0.45
5,7-Dimethoxycoumarin	206.197	1.8102	0.24	0.17
Isopimpinellin	246.218	2.5564	0.36	0.35
Nomilin	514.571	3.6902	0.12	0.24
Obacunone	454.519	3.9246	0.15	0.41
1-Palmitoyl-2-hydroxy-sn-glycero-3-phosphoethanolamine	469.556	4.9614	0.08	0.68
1-Palmitoyl-sn-glycero-3-phosphocholine	496.646	5.2116	0.02	0.80
Esculetin	178.143	1.2042	0.24	0.71
1-Oleoyl-sn-glycero-3-phosphocholine	522.684	5.7678	0.06	0.85
Cinnamic acid	148.161	1.7844	0.01	0.51
8-Allyloxypsoralen	242.23	3.104	0.35	0.39
3-Propyl-2-methylpyrazine	136.198	1.73752	0.14	0.77
Xanthotoxol	202.165	2.2448	0.15	0.68
Bergaptol	202.165	2.2448	0.19	0.59
Bergamotin	338.403	5.6107	0.30	0.46
5-Geranoxy-7-methoxy-coumarin	328.408	4.8731	0.25	0.31
8-O-Acetylharpagide	406.384	-2.8934	0.13	0.17

Several of the phytochemicals listed in **Table 1** fall within the physicochemical ranges generally considered favorable for topical application. Small phenolic compounds and coumarins, such as xanthotoxol (MW: 202.165 Da, Log P: 2.2448), heraclenin (MW: 286.283 Da, Log P: 3.0954), and 7-methoxycoumarin (MW: 176.171 Da, Log P: 1.8016), meet the predefined molecular weight and Log P criteria. Several flavonoids identified in the peel, including luteolin (MW: 286.239 Da, Log P: 2.2824), quercetin (MW: 302.238 Da, Log P: 1.988), and hesperetin (MW: 302.282 Da, Log P: 2.5185), also fall within these ranges. The limonoids limonin (MW: 470.518 Da, Log P: 3.1374) and obacunone (MW: 454.519 Da, Log P: 3.9246) have molecular weights close to the upper limit but remain within the selected Log P range, suggesting favorable physicochemical properties for skin partitioning.

The AMES and skin reaction predictions in **Table 1** provide additional information on the potential safety of these compounds. The AMES prediction is related to the potential mutagenic effect, while the skin reaction prediction indicates the possibility of an adverse skin response. Xanthotoxol and obacunone showed relatively low AMES prediction values (0.15), although their skin reaction values differed (0.68 and 0.41, respectively). Luteolin and quercetin showed favorable molecular weight and Log P values but had relatively high skin reaction values (0.88 and 0.89, respectively). These findings suggest that their potential skin tolerability should be considered when developing a topical formulation. In addition, luteolin has been reported to reduce MMP-9and TNF-α expression in diabetic wound models and to promote re-epithelialization (26,27), supporting its potential relevance for wound-healing applications.

Several compounds in **Table 1** were excluded during the initial physicochemical screening because their molecular weights exceeded 500 Da or their Log P values fell outside the selected range. Glycosylated flavonoids such as rutin (MW: 610.521 Da),

diosmin (MW: 608.549 Da), and hesperidin (MW: 610.565 Da) exceeded the molecular weight limit and showed negative Log P values, indicating limited suitability for passive skin permeation. Similarly, citric acid and trans-aconitic acid had negative Log P values (-1.2485 and -0.4433, respectively), suggesting limited partitioning into the lipid-rich stratum corneum despite their relatively low molecular weights. These compounds may therefore require additional formulation strategies, such as permeation enhancers or physical delivery approaches, to improve their penetration into the skin (28,29).

3.2 Molecular docking

Molecular docking analysis was performed to quantitatively assess the predicted binding affinities of phytochemicals from *Citrus aurantiifolia* for matrix metalloproteinase-9 (MMP-9) and tumor necrosis factor-alpha (TNF-α), which are two key targets in chronic wounds *(30,31)*. Before proceeding to the docking result, redocking of native ligands from both receptors was performed to validate the molecular docking procedure. Based on Figure 1, the RMSD values for MMP-9 (1.655 Å) and TNF-α (1.210 Å) are lower than 2 Å, meaning the docking method is validated.

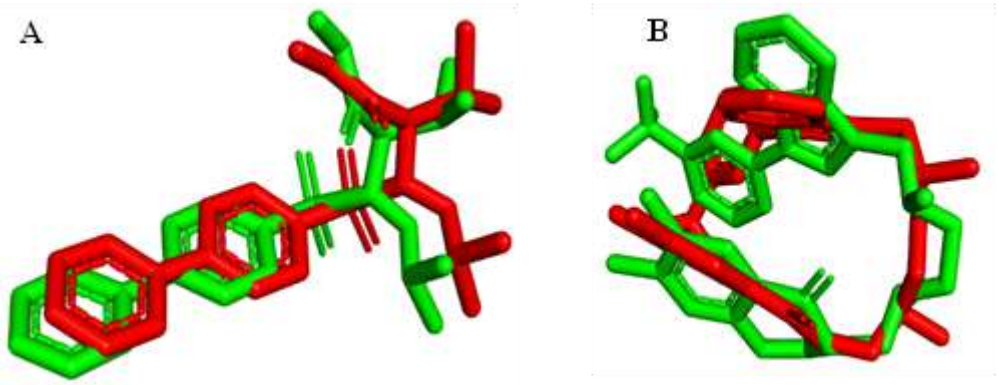

Figure 1. The overlay of native ligand before (red) and after (green) the redocking procedure of MMP-9 (A) and TNF-α (B).

As shown in **Table 2**, several bioactive compounds displayed binding affinities significantly higher than both the native ligands and the pharmaceutical standard doxycycline (1). In particular, compounds like 3'-hydroxygenkwanin, luteolin, obacunone, and limonin have shown to be the best candidates with promising thermodynamic profiles with binding energies as low as -10.3 kcal/mol. Visual analysis (**Figure 2**) confirms that all lime-derived compounds targeted the same primary active site in both proteins with the exception of doxycycline in MMP-9, which occupied a different pocket. This strong competition for the catalytic sites indicates an effective way to reduce the excessive activity of protease and cytokines.

Table 2. The investigation of binding affinity values from compounds of *C. aurantiifolia* fot MMP-9 and TNF-α.

Compounds	Binding affinity (kcal/mol)	
	MMP-9	TNF-α
limonin	-8.2	-10
luteolin	-10	-7.8
3`-hydroxygenkwanin	-10.1	-7.7
myricetin	-9.2	-7.7
europetin	-9.1	-7.4
2-(Methylthio)benzothiazole	-7.0	-5.2
Phenprobamate	-7.4	-5.6

trans-3-Coumaric acid	-7.6	-5.8
cis-3-Coumaric acid	-7.3	-5.7
Quercetin	-9.5	-7.7
Quercetin 3'-methyl ether	-9.4	-7.4
Hesperetin	-7.0	-7.3
Mono-2-ethylhexyl phthalate	-7.0	-6.3
Scoparone	-8.1	-5.9
Heraclenin	-8.1	-7.5
Oxypeucedanin hydrate	-7.0	-7.3
Byakangelicol	-8.4	-7.2
7-Methoxycoumarin	-8.1	-5.8
Angelicin	-8.7	-6.9
5,7-Dimethoxycoumarin	-6.1	-5.9
Isopimpinellin	-6.6	-6.8
Obacunone	-10.3	-9.1
1-Palmitoyl-2-hydroxy-sn-glycero-3-phosphoethanolamine	-6.7	-5.4
Esculetin	-7.9	-6.1
Cinnamic acid	-7.1	-5.8
8-Allyloxypsoralen	-7.8	-7.0
3-Propyl-2-methylpyrazine	-6.0	-5.0
Xanthotoxol	-9.8	-6.8
Bergaptol	-9.0	-6.6
5-Geranoxy-7-methoxy-coumarin	-8.1	-7.7
Native ligand	-9.5	-8.6
Doxycycline	-7.6	-8.0

The candidates showed excellent stability through key residue interactions for the target MMP-9 responsible for excess collagen degradation in non-healing wounds. **Table 3** demonstrated that 3'-hydroxygenkwanin (-10.1 kcal/mol) and obacunone (-10.3 kcal/mol) interacted strongly with His226, a crucial residue that coordinates the catalytic zinc ion that is necessary for enzyme function. Moreover, both compounds formed hydrogen bonds with Tyr248, an important stabilizer of the catalytic pocket (32,33). The profile of Luteolin (-10.0 kcal/mol) was further supported by hydrophobic interactions with Leu188, Val223, and Tyr248 in addition to hydrogen bonding with Ala189. These interactions may contribute to the inhibition of MMP-9 by interfering with key catalytic and substrate-binding residues, including His226 and Tyr248, thus preventing overactive proteolysis of the extracellular matrix (ECM) and thereby protecting the structural integrity of new tissue and allowing transition into the remodeling phase (34).

Natural Resources for Human Health
eISSN: 2583-1194

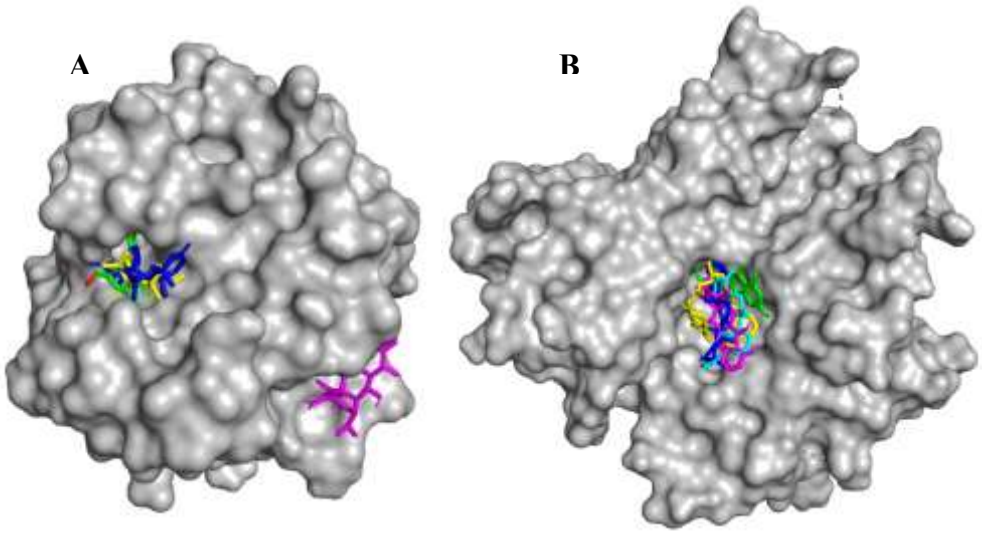

Figure 2. 3D visualization of the potential compounds, native ligands (yellow), and Doxycycline (purple) interacting with the active sites of MMP-9(a) and TNF-α (b). 3'-Hydroxygenkwanin (red), Luteolin (green), Obacunone (blue), and Limonin (cyan). The observed interactions suggest potential inhibition of MMP-9 and TNF-α activity.

In the inflammatory phase, the compounds showed high potency to interfere with the activity of TNF-α, a major contributor to persistent wound inflammation. Limonin had a strong binding ability of -10.0 kcal/mol by creating a hydrogen bond with Gly121 and interacting with Leu57 and Tyr151 in a way that avoids water. Both obacunone and luteolin targeted the hydrophobic residue Tyr119, which is essential for the formation and stabilization of the active TNF-α structure (35,36). Obacunone specifically interacts with Tyr59 and Tyr119 through hydrophobic contacts, while luteolin connects with Ser60 and Leu120 using hydrogen bonds. A higher number of hydrogen bonds means a stable formed complex because this type of interaction is very strong (37). These phytochemicals, by binding to these essential residues, particularly Tyr119, may prevent the assembly of the functional cytokine structure, thereby reducing the production of pro-inflammatory signals (38). This anti-inflammatory effect provides a protected environment to support cellular proliferation and increases the rate of overall wound healing.

Table 3. List of interactions of ligands of *C. aurantiifolia* toward MMP-9 and TNF-α receptor.

Compounds	MMP-9		TNF-α	
	Hydrophobic	Hydrogen Bond	Hydrophobic	Hydrogen Bond
3'hydroxygenkwanin	Leu188, Ala189, Val223, His226	Gly186, Tyr248	Tyr119	Gly121
luteolin	Leu188, Val223, His226, Tyr248	Ala189, Leu243	Tyr119	Ser60, Leu120
obacunone	Val223, His226	Tyr248	Tyr59, Tyr119	-
limonin	Asp165, His118	His117	Leu57, Tyr151	Gly121
the native ligand	Val223, His226, Tyr248	Leu188, Ala189	Leu57, Tyr59, Tyr119, Gly121	-
doxycycline	Pro196	Asp165, Ile198, Asp201	Ser60, Leu120, Gly121, Tyr151	Tyr151

The choice of these compounds for further molecular dynamics (md) analysis is based on their high binding potency and their suitable physicochemical properties for topical delivery. Unlike many potent flavonoids that are too large for passive diffusion, some candidates such as luteolin, obacunone, and 3'-hydroxygenkwanin have molecular weights below 500 g/mol and favorable log p values. Biologically, luteolin has been shown to reduce the protein expression of MMP-9 and TNF-α in vivo, which has a direct relationship with improved wound closure (26,27). These combined docking results **(table 2**) and interaction profiles **(table 3)** show that these compounds derived from lime are highly promising candidates for the development of targeted topical wound therapies.

3.3. Molecular Dynamic Study

The molecular dynamics (MD) simulation results for the lead bioactive compounds from *C. aurantiifolia* offer a quantitative evaluation of their thermodynamic stability and conformational integrity in the catalytic sites of MMP-9 and TNF-α over a 50 ns trajectory.

As shown in **Figure 3,** for the MMP-9 target, the RMSD profiles of the 3'-hydroxygenkwanin and luteolin complexes show a very stable binding mode (below 3 Å), with both systems reaching equilibrium after approximately 30 ns and maintaining average deviation values of 2.5 Å (39). However, obacunone showed much higher fluctuations, with rmsd values reaching around 10 Å toward the end of the simulation. This increased deviation indicates that obacunone has the highest initial binding affinity, but its complex with MMP-9exhibits significant structural adaptation or conformational changes in the catalytic domain over time. The radius of gyration (Rg) for MMP-9 was highly stable for 3'- hydroxygenkwanin (~14.8 Å) and luteolin (~14.7 Å), implying that these compounds will maintain the protein in a compact, functionally inhibited form over the entire simulated period.

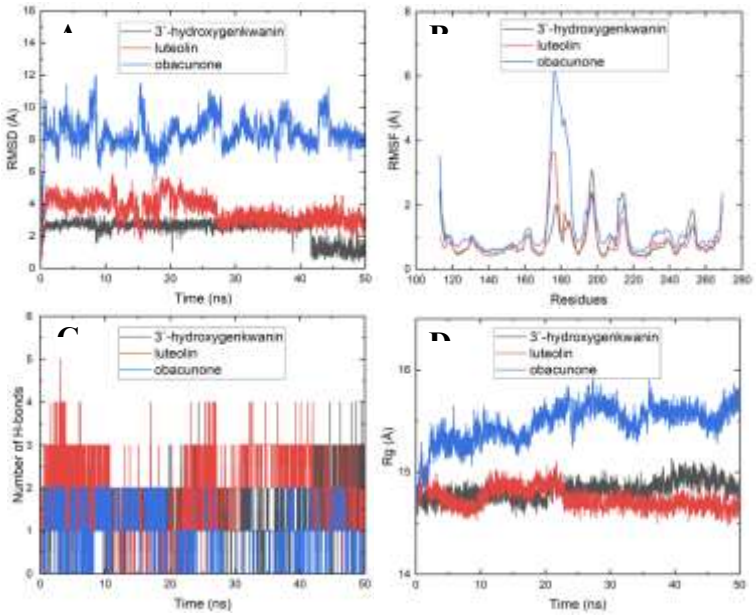

Figure 3. Molecular dynamics simulation results of potential *C. aurantiifolia* compounds for MMP-9 inhibition, including RMSD (A), RMSF (B), hydrogen bond number (C), and radius of gyration (Rg) (D).

MD results in the context of TNF-α inhibition show that all candidates, including limonin, luteolin, and obacunone, have rmsd values in the range of 7 Å and 10 Å **(Figure 4A).** Among the TNF-α inhibitors, obacunone showed the most stable profile, reaching a plateau at an average of 7.8 Å (**Figure 4A),** while limonin showed the largest deviations, approaching 10 Å. However, the Rg for all TNF-α complexes remained stable in the range of 18.8 Å to 19.3 Å **(Figure 4D),** despite these fluctuations, confirming the preservation of the overall protein structure. These stability measures suggest that these lime-derived compounds can interact with the TNF-α subunit interface, potentially interfering with functionally relevant inter-subunit interactions and thereby attenuating the signaling cascade that contributes to chronic inflammation.

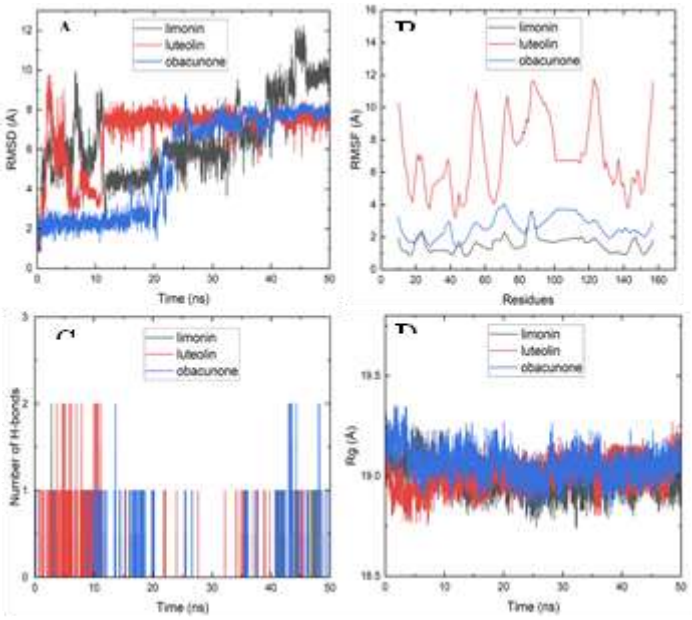

Figure 4. The molecular dynamic trajectory result from potential compounds of *C. aurantiifolia* inhibiting TNF-α, including RMSD (A), RMSF (B), hydrogen bond number (C), and gyrate (D).

The RMSF analysis provided a detailed assessment of individual residue flexibility within a single TNF-α subunit (residues 10–157) upon phytochemical binding (40). In the MMP-9 MD simulation, the residues (200–230) of the active site, which contains the important his226 zinc-coordination site, had little fluctuation (<1.0 Å) for the 3'-hydroxygenkwanin and luteolin complexes **(figure 3B).** This immobilization of the catalytic core is a key signature for the durable inhibition of the enzyme. Likewise, the residues forming the hydrophobic binding pocket in the TNF-α complexes, particularly the tyr119, showed decreased mobility compared to the surrounding loops. Luteolin showed more overall fluctuations in the terminal loop regions of the cytokine, but the molecular docking data support its persistent occupancy of the subunit interface, validating its role as a potent anti-inflammatory agent that facilitates the transition of wounds into the proliferative phase.

The analysis of hydrogen bond frequency and hydrophobic contacts further supported the stability of these protein–ligand interactions. 3'-hydroxygenkwanin and luteolin formed a stable network of 1 to 3 hydrogen bonds in the MMP-9 complexes throughout the 50 ns simulation, validating the binding energy seen in the initial docking (**Figure 3C**). Frequent interactions with residues such as Tyr248 and Gly186 may help maintain the potential inhibitor within the S1' pocket, thereby potentially interfering with collagen substrate access to the catalytic site (41). In contrast, TNF-α binders showed a higher dependence on hydrophobic interaction for the stability of the formed complex, as indicated by the limited data on hydrogen bonding, usually in the range of 0 to 1. This mechanism is consistent with current knowledge that small molecule TNF-α inhibitors act by binding to the internal hydrophobic core of the active site and blocking subunit assembly (37,42). Overall, the MD results support 3'-hydroxygenkwanin and luteolin as structurally stable MMP-9-binding candidates, while limonin, luteolin, and obacunone showed favorable interactions with the TNF-α interface. Together with the docking results, these findings highlight the potential of these phytochemicals as candidates for further investigation of protease and cytokine inhibition in chronic wound management. Among the evaluated compounds, 3'-hydroxygenkwanin showed a particularly favorable predicted binding affinity for MMP-9, whereas limonin and obacunone exhibited favorable predicted binding profiles for both targets.

4. CONCLUSION

The in silico analysis identified several non-volatile constituents of Citrus aurantiifolia peel with favorable predicted binding affinities for MMP-9and TNF-α. The docking protocol was validated through redocking of the native ligands, yielding RMSD values below 2.0 Å. Obacunone and limonin exhibited more favorable predicted binding affinities than doxycycline for both targets, suggesting their potential as dual-target candidates for further investigation. At the MMP-9catalytic site, 3'-hydroxygenkwanin and luteolin demonstrated favorable binding interactions and maintained relatively stable complexes during molecular dynamics simulations. In comparison, limonin and obacunone showed the most favorable predicted binding affinities

for TNF-α. Overall, these findings provide a basis for further experimental evaluation of selected C. aurantiifolia phytochemicals as potential components of topical formulations for chronic wound management.

AUTHOR CONTRIBUTIONS

Imam Adrian Rakhman: Conceptualization, Investigation.

Imam Adrian Rakhman, Syahrijuita Kadir: Methodology, Laboratory Analysis.

Ilhamuddin: Data Curation, Formal Analysis.

Gita Vita Soraya: Supervision, Writing—Review & Editing.

CONFLICT OF INTEREST

The authors declare that there is no conflict of interest.

ETHICS STATEMENT

Ethical approval was not required for this study as it was conducted purely *in silico* using publicly available databases, without the involvement of human participants or animal subjects.

DATA AVAILABILITY STATEMENT

The data supporting the findings of this study were obtained from publicly available databases, specifically the Protein Data Bank (https://www.rcsb.org/) and PubChem (https://pubchem.ncbi.nlm.nih.gov/).

REFERENCES

[1] 1.Jing SL, Suh EJ, Huang KX, Griffin MF, Wan DC, Longaker MT. Understanding and Advancing Wound Healing in the Era of Multi-Omic Technology. Bioengineering. 2026 Jan;13(1):51. doi:10.3390/bioengineering13010051

[2] 2.Aitcheson SM, Frentiu FD, Hurn SE, Edwards K, Murray RZ. Skin Wound Healing: Normal Macrophage Function and Macrophage Dysfunction in Diabetic Wounds. Molecules. 2021 Aug 13;26(16):4917. doi:10.3390/molecules26164917 PubMed PMID: 34443506; PubMed Central PMCID: PMC8398285.

[3] 3.Avishai E, Yeghiazaryan K, Golubnitschaja O. Impaired wound healing: facts and hypotheses for multi-professional considerations in predictive, preventive and personalised medicine. EPMA Journal. 2017 Mar 1;8(1):23–33. doi:10.1007/s13167-017-0081-y

[4] 4.Caley MP, Martins VLC, O'Toole EA. Metalloproteinases and Wound Healing. Adv Wound Care (New Rochelle). 2015 Apr 1;4(4):225–34. doi:10.1089/wound.2014.0581 PubMed PMID: 25945285; PubMed Central PMCID: PMC4397992.

[5] 5.Ågren MS, Schnabel R, Christensen LH, Mirastschijski U. Tumor necrosis factor-α-accelerated degradation of type I collagen in human skin is associated with elevated matrix metalloproteinase (MMP)-1 and MMP-3 ex vivo. European Journal of Cell Biology. 2015 Jan 1;94(1):12–21. doi:10.1016/j.ejcb.2014.10.001

[6] 6.Rodrigues KE, Pontes MHB, Cantão MBS, Prado AF. The role of matrix metalloproteinase-9 in cardiac remodeling and dysfunction and as a possible blood biomarker in heart failure. Pharmacological Research. 2024 Aug 1;206:107285. doi:10.1016/j.phrs.2024.107285

[7] 7.Mäkelä M, Salo T, Larjava H. MMP-9from TNF alpha-stimulated keratinocytes binds to cell membranes and type I collagen: a cause for extended matrix degradation in inflammation? Biochem Biophys Res Commun. 1998 Dec 18;253(2):325–35. doi:10.1006/bbrc.1998.9641 PubMed PMID: 9878537.

[8] 8.Coondoo A, Phiske M, Verma S, Lahiri K. Side-effects of topical steroids: A long overdue revisit. Indian Dermatol Online J. 2014;5(4):416–25. doi:10.4103/2229-5178.142483 PubMed PMID: 25396122; PubMed Central PMCID: PMC4228634.

[9] 9.Yasir M, Goyal A, Sonthalia S. Corticosteroid Adverse Effects. In: StatPearls [Internet]. Treasure Island (FL): StatPearls Publishing; 2026 [cited 2026 May 24]. Available from: http://www.ncbi.nlm.nih.gov/books/NBK531462/ PubMed PMID: 30285357.

[10] 10.Barba-Ostria C, Carrera-Pacheco SE, Gonzalez-Pastor R, Heredia-Moya J, Mayorga-Ramos A, Rodríguez-Pólit C, et al. Evaluation of Biological Activity of Natural Compounds: Current Trends and Methods. Molecules. 2022 Jul 13;27(14):4490. doi:10.3390/molecules27144490 PubMed PMID: 35889361; PubMed Central PMCID: PMC9324072.

[11] 11.Esad M, Dimov I, Choneva M, Popova M, Kokova V, Apostolova E, et al. Molecular Mechanisms of Wound Healing: The Role of Medicinal Plants. Life (Basel). 2025 Nov 14;15(11):1748. doi:10.3390/life15111748 PubMed PMID: 41302172; PubMed Central PMCID: PMC12653338.
[12] 12.K M, Sm S. The effectiveness of polyherbal formulations in regenerating wounds and profiling their therapeutic properties was tracked via high-throughput methods in conjunction with In silico molecular docking. Phytomedicine Plus. 2026 Feb 1;6(1):100950. doi:10.1016/j.phyplu.2025.100950
[13] 13.Alberts A, Lungescu IA, Niculescu AG, Grumezescu AM. Natural Products for Improving Soft Tissue Healing: Mechanisms, Innovations, and Clinical Potential. Pharmaceutics. 2025 Jun;17(6):758. doi:10.3390/pharmaceutics17060758
[14] 14.Elmaidomy AH, Abdelmohsen UR, Sayed AM, Altemani FH, Algehainy NA, Soost D, et al. Antiplasmodial potential of phytochemicals from Citrus aurantiifolia peels: a comprehensive in vitro and in silico study. BMC Chemistry. 2024 Mar 30;18(1):60. doi:10.1186/s13065-024-01162-x
[15] 15.Phucharoenrak P, Muangnoi C, Trachootham D. Metabolomic Analysis of Phytochemical Compounds from Ethanolic Extract of Lime (Citrus aurantiifolia) Peel and Its Anti-Cancer Effects against Human Hepatocellular Carcinoma Cells. Molecules. 2023 Jan;28(7):2965. doi:10.3390/molecules28072965
[16] 16.Rajendran P, Rathinasabapathy R, Chandra Kishore S, Bellucci S. Computational-Simulation-Based Behavioral Analysis of Chemical Compounds. Journal of Composites Science. 2023 May;7(5):196. doi:10.3390/jcs7050196
[17] 17.Abookleesh F, Mosa FES, Barakat K, Ullah A. Assessing Molecular Docking Tools to Guide the Design of Polymeric Materials Formulations: A Case Study of Canola and Soybean Protein. Polymers. 2022 Jan;14(17):3690. doi:10.3390/polym14173690
[18] 18.Swanson K, Walther P, Leitz J, Mukherjee S, Wu JC, Shivnaraine RV, et al. ADMET-AI: a machine learning ADMET platform for evaluation of large-scale chemical libraries. Bioinformatics. 2024 Jul 1;40(7):btae416. doi:10.1093/bioinformatics/btae416
[19] 19.Forli S, Huey R, Pique ME, Sanner M, Goodsell DS, Olson AJ. Computational protein-ligand docking and virtual drug screening with the AutoDock suite. Nat Protoc. 2016 May;11(5):905–19. doi:10.1038/nprot.2016.051 PubMed PMID: 27077332; PubMed Central PMCID: PMC4868550.
[20] 20.Rao P, Shukla A, Parmar P, Rawal RM, Patel B, Saraf M, et al. Reckoning a fungal metabolite, Pyranonigrin A as a potential Main protease (Mpro) inhibitor of novel SARS-CoV-2 virus identified using docking and molecular dynamics simulation. Biophysical Chemistry. 2020 Sep 1;264:106425. doi:10.1016/j.bpc.2020.106425
[21] 21.Sucahyo A, Rahman MF, Khotimah H, Widodo W, Ulfa SM. Identification of flavone and flavanone from ethyl acetate fraction of Caesalpinia sappan heartwood and tentative structure-activity relationship: An in vitro and in silico approach. J App Pharm Sci. 2023 Nov 4;13,(11):089–100. doi:10.7324/JAPS.2023.92856
[22] 22.Hmingthansanga V, Singh N, Banerjee S, Manickam S, Velayutham R, Natesan S. Improved Topical Drug Delivery: Role of Permeation Enhancers and Advanced Approaches. Pharmaceutics. 2022 Dec 15;14(12):2818. doi:10.3390/pharmaceutics14122818 PubMed PMID: 36559311; PubMed Central PMCID: PMC9785322.
[23] 23.Bultum LE, Tolossa GB, Kim G, Kwon O, Lee D. In silico activity and ADMET profiling of phytochemicals from Ethiopian indigenous aloes using pharmacophore models. Sci Rep. 2022 Dec 23;12(1):22221. doi:10.1038/s41598-022-26446-x
[24] 24.Dmitriev AV, Lagunin AA, Rudik AV, Savosina PI, Druzhilovskiy DS, Filimonov DA, et al. SAR Modeling to Predict Ames Mutagenicity Across Different Salmonella typhimurium Strains. Pharmaceuticals. 2025 Dec;18(12):1853. doi:10.3390/ph18121853
[25] 25.de Groot A. Allergic Contact Dermatitis from Topical Drugs: An Overview. Dermatitis®. 2021 Aug 1;32(4):197–213. doi:10.1097/DER.0000000000000737
[26] 26.Gendrisch F, Esser PR, Schempp CM, Wölfle U. Luteolin as a modulator of skin aging and inflammation. BioFactors. 2021;47(2):170–80. doi:10.1002/biof.1699
[27] 27.Chen LY, Cheng HL, Kuan YH, Liang TJ, Chao YY, Lin HC. Therapeutic Potential of Luteolin on Impaired Wound Healing in Streptozotocin-Induced Rats. Biomedicines. 2021 Jun 30;9(7):761. doi:10.3390/biomedicines9070761 PubMed PMID: 34209369; PubMed Central PMCID: PMC8301369.

[28] 28.Nguyen HX, Nguyen CN. Microneedle-Mediated Transdermal Delivery of Biopharmaceuticals. Pharmaceutics. 2023 Jan 13;15(1):277. doi:10.3390/pharmaceutics15010277 PubMed PMID: 36678906; PubMed Central PMCID: PMC9864466.
[29] 29.Fantini A, Delledonne A, Casula L, Nicoli S, Pescina S, Cardia MC, et al. Application of Microneedles for High-Molecular-Weight Dextran Penetration Across the Buccal Mucosa. Pharmaceuticals. 2025 Feb;18(2):158. doi:10.3390/ph18020158
[30] 30.Al-Roub A, Akhter N, Al-Rashed F, Wilson A, Alzaid F, Al-Mulla F, et al. TNFα induces matrix metalloproteinase-9 expression in monocytic cells through ACSL1/JNK/ERK/NF-kB signaling pathways. Sci Rep. 2023 Sep 1;13:14351. doi:10.1038/s41598-023-41514-6 PubMed PMID: 37658104; PubMed Central PMCID: PMC10474281.
[31] 31.Yuan Y, Yang Y, Ji Z, Feng J, Shu L, Xiao S, et al. Wound microenvironment sensing and self-adjusting hydrogel with glucose, ROS, and MMP-9responsiveness for improving microcirculation of diabetes foot ulcers. Chemical Engineering Journal. 2025 Feb 1;505:159537. doi:10.1016/j.cej.2025.159537
[32] 32.Istyastono EP, Yuniarti N, Prasasty VD, Mungkasi S, Waskitha SSW, Yanuar MRS, et al. Caffeic Acid in Spent Coffee Grounds as a Dual Inhibitor for MMP-9and DPP-4 Enzymes. Molecules. 2023 Oct 19;28(20):7182. doi:10.3390/molecules28207182 PubMed PMID: 37894660; PubMed Central PMCID: PMC10609219.
[33] 33.Malekipour MH, Shirani F, Moradi S, Taherkhani A. Cinnamic acid derivatives as potential matrix metalloproteinase-9 inhibitors: molecular docking and dynamics simulations. Genomics Inform. 2023 Mar 31;21(1):e9. doi:10.5808/gi.22077 PubMed PMID: 37037467; PubMed Central PMCID: PMC10085732.
[34] 34.Ballav S, Lokhande KB, Dabhi I, Inje S, Ranjan A, Swamy KV, et al. Designing Novel Quercetin Derivatives as Matrix Metalloproteinase-9 Inhibitors in Colon Carcinoma: An: In vitro: and: In silico: Approach. Journal of Dental Research and Review. 2020 Feb;7(Suppl 1):S30. doi:10.4103/jdrr.jdrr_67_19
[35] 35.Zia K, Ashraf S, Jabeen A, Saeed M, Nur-e-Alam M, Ahmed S, et al. Identification of potential TNF-α inhibitors: from in silico to in vitro studies. Sci Rep. 2020 Dec 1;10:20974. doi:10.1038/s41598-020-77750-3 PubMed PMID: 33262408; PubMed Central PMCID: PMC7708426.
[36] 36.Ahmed EA, Rajendran P, Adam MSS, Abdelsalam S. Marine algal TNF-α inhibitors explored by comparative docking and molecular dynamics simulations. Computational Biology and Chemistry. 2026 Oct 1;124:109059. doi:10.1016/j.compbiolchem.2026.109059
[37] 37.Zia K, Ashraf S, Jabeen A, Saeed M, Nur-e-Alam M, Ahmed S, et al. Identification of potential TNF-α inhibitors: from in silico to in vitro studies. Sci Rep. 2020 Dec 1;10(1):20974. doi:10.1038/s41598-020-77750-3
[38] 38.Seo H, Haseeb M, Choi S. Structural and molecular characterization of a small-molecule TNF-α–TNFR1 inhibitor modulating cell death signaling. Biochemical Pharmacology. 2026 Apr 1;246:117727. doi:10.1016/j.bcp.2026.117727
[39] 39.Nafisah W, Fatchiyah F, Widyananda M, Christina Y, Djati M, Widodo N, et al. Potential of bioactive compound of Cyperus rotundus L. rhizome extract as inhibitor of PD-L1/PD-1 interaction: An in silico study AGRICULTURE AND NATURAL RESOURCES. Agriculture and Natural Resources. 2022 Jan 1;751–60. doi:10.34044/j.anres.2022.56.4.09
[40] 40.Othman B, Beigh S, Albanghali MA, Sindi AAA, Shanawaz MA, Ibahim MAEM, et al. Comprehensive pharmacokinetic profiling and molecular docking analysis of natural bioactive compounds targeting oncogenic biomarkers in breast cancer. Sci Rep. 2025 Feb 13;15(1):5426. doi:10.1038/s41598-024-84401-4
[41] 41.Li Z, Wei J, Chen B, Wang Y, Yang S, Wu K, et al. The Role of MMP-9and MMP-9Inhibition in Different Types of Thyroid Carcinoma. Molecules. 2023 Apr 25;28(9):3705. doi:10.3390/molecules28093705 PubMed PMID: 37175113; PubMed Central PMCID: PMC10180081.
[42] 42.Chan DSH, Lee HM, Yang F, Che CM, Wong CCL, Abagyan R, et al. Structure-Based Discovery of Natural Product-Like TNF-α Inhibitors. Angew Chem Int Ed Engl. 2010 Apr 6;49(16):2860–4. doi:10.1002/anie.200907360 PubMed PMID: 20235259; PubMed Central PMCID: PMC4162403.